Silver-Coated Engineered Magnetic Nanoparticles Are Promising for the Success in the Fight against Antibacterial Resistance Threat

Morteza Mahmoudi[†,‡,*] and Vahid Serpooshan[§]

[†]Nanotechnology Research Center, Faculty of Pharmacy, Tehran University of Medical Sciences, Tehran, Iran, [‡]National Cell Bank, Pasteur Institute of Iran, #69 Pasteur Avenue, Tehran 13164, Iran, and [§]Division of Pediatric Cardiology, Department of Pediatrics, Stanford University School of Medicine, Stanford, California 94305-5101, United States

ABSTRACT The combination of patients with poor immune system, prolonged exposure to anti-infective drugs, and cross-infection has given rise to nosocomial infections with highly resistant pathogens, which is going to be a growing threat so termed "antibiotic resistance". Due to their significant antimicrobial activity, silver nanoparticles are recognized as a promising candidate to fight against resistant pathogens; however, there are two major shortcomings with these nanoparticles. First, the silver nanoparticles are highly toxic to the healthy cells; second, due to the protection offered by the biofilm mode of growth, the silver nanoparticles cannot eradicate bacterial biofilms. In order to overcome these limitations, this study introduces a new class of engineered multimodal nanoparticles comprising a magnetic core and a silver ring with a ligand gap. The results indicated promising capability of the designed multimodal nanoparticles for high-yield antibacterial effects and eradication of bacterial biofilms, while the particles were completely compatible with the cells. Utilizing a gold ring as an intermediate coating on the produced nanoparticles may exploit new opportunities for theranosis applications. This will require special consideration in future works.

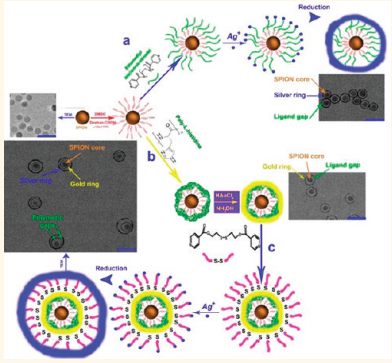

KEYWORDS: antibiotic resistance · silver nanoparticles · magnetic nanoparticles · toxicity · biofilm · ligand gap

Antibiotics have been long known as "miraculous drugs" to cure fatal infectious diseases and have been excessively used even without medical doctors' prescriptions. The inappropriate and disproportionate use of antibacterial drugs (*e.g. Staphylococcus aureus* infections treatment by the drug penicillin) in humans and also in veterinary and agricultural medicine has led to a rapid increase in the prevalence of drug-resistant micro-organisms.[1] The most catastrophic effect of antibiotic resistance is the emergence of new bacterial strains which are resistant to numerous antibiotics simultaneously. The new infections caused by these multi-drug-resistant pathogens can dramatically aggravate the clinical complications. They can also cause a higher risk of serious diseases that could have been readily treated, longer hospital stays, and, hence, considerably greater expenses for the society. In the most severe circumstance, which regrettably is not unlikely, the incompetence of the employed antibiotics to the new dangerous pathogens can cause uncontrolled epidemics of bacterial diseases that can no longer be treated.

Pathogenic infections that are associated with biomaterials are another critical issue in this context. The average life expectancy in human society has been gradually increasing, resulting in higher demands for the replacement of organs (tissues) by biomaterials in elderly people. Consequently, the use of biomaterial implants (*e.g.*, artificial tissues) will be extensively increasing. The pathogenic infections can be initiated by peri-operative bacterial contamination of the graft surface during implantation, immediately postsurgery, during hospitalization, or through hematogenous spreading of bacteria from infections elsewhere in the body.[2] In general, *Staphylococcus epidermidis* and *Staphylococcus aureus* are the most frequently isolated pathogens from infected biomaterial implants. Approximately, 50% of infection associated with catheters, artificial joints, and heart valves are caused by *Staphylococcus epidermidis*,[3] whereas *Staphylococcus aureus* is detected in ~23%

* Address correspondence to mahmoudi@biospion.com.

Received for review January 4, 2012 and accepted February 21, 2012.

Published online March 07, 2012
10.1021/nn300042m

of the infections associated with prosthetic joints.[3] *Staphylococcus epidermidis* and *Staphylococcus aureus* often protect themselves against antibiotics and the host immune system *via* producing a matrix of exopolymeric substances that embed the organisms in a matrix, impenetrable for the most antibiotics and immune cells. Accordingly, in order to increase the efficacy of antibiotics, the alternative drugs should have the ability to infiltrate the biofilm.

Nowadays, nanotechnology has turned into a keyword of public interest, and a part of our daily life, as the social and economic impact of nanotechnological developments is being recognized. However, there are still several unknown aspects of the widespread application of the nanosciences in human life, in the fields including novel materials manufacturing, electronics, cosmetics, pharmaceutics, and medicine.[4] During the past decade, the application of nanomaterials in medicine significantly increased, which resulted in raising hopes for employing nanoparticles as alternative antibiotic agents.[5] Among various types of nanoparticles, silver nanoparticles are well-recognized as promising antimicrobial agents.[6] However, there are two major shortcomings with these particles: (1) their toxic effects on human cells and (2) their low yield for penetration through the bacterial biofilms.[7−9]

In this study, we demonstrated that a novel class of ultrathin (∼1−2 nm) silver ring-coated superparamagnetic iron oxide nanoparticles (SPIONs) with ligand gaps exhibit strong antimicrobial characteristics against bacteria while maintaining remarkable compatibility with the cells. Moreover, ultrathin (∼1−2 nm) silver ring-coated intermediate gold-coated SPIONs with double ligand gaps were developed that can be potentially used as multimodal antibacterial agents. Due to their magnetic core, both nanoparticles are able to deeply penetrate in the bacterial biofilms when an external magnetic field is applied, resulting in a high therapeutic index against *Staphylococcus epidermidis* and *Staphylococcus aureus* infections. Taken together, silver ring-engineered magnetic nanoparticles are promising antimicrobial agents that can be used to treat infectious diseases. These nanoparticulate systems can be future improved to avoid antibiotic resistance, owing to their multi-antibiotic capabilities with extensive changeable physicochemical properties.

RESULTS AND DISCUSSION

Figure 1 illustrates the schematic representation of the major steps involved in producing various silver ring SPIONs. Monodispersed hydrophobic SPIONs were first immersed in dimethyl sulfoxide (DMSO) in the presence of carboxylated dextran, resulting in the assembly of hydrophilic coated SPIONs *via* ligand exchange phenomenon. Ethanediylbis(isonicotinate) was then adsorbed onto the outer surface of carboxylated dextran-coated particles through charge−charge interaction. The distinguished characteristic of the ethanediylbis(isonicotinate) polymer is its ability to absorb silver ions on the outer surface of nanoparticles at a high packing density. The main function of multilayer organic molecules (carboxylate dextran and ethanediylbis(isonicotinate)), deposited on the surface of SPIONs, is to allow the direct growth of silver ions on the core of nanoparticles. These silver ions, in turn, give rise to the barrier preventive characteristic of the coated SPIONs. Further reduction of the highly packed silver ions, trapped at the surface of the SPION, by a reducing reagent leads to the formation of SPION−silver core−shell nanoparticles with clear ligand gaps (see the inset in Figure 1a). The obtained particles are proposed to have suitable magnetic properties, due to the existence of SPION as the core, and antibacterial effects, due to the presence of a thin layer of silver as the shell.

The function of the manufactured nanoparticles can be further augmented to meet the properties required in diverse applications. For example, surface-enhanced Raman scattering (SERS)-based signal amplification and detection can be utilized to prepare nanoparticles suitable for molecular imaging and sensing applications. This study introduced a high-yield synthetic method for the preparation of SERS-active SPION−gold−silver, core−intermediate shell−shell multifunctional nanoparticles. The particles possess two ligand gaps located between core−intermediate shell and intermediate shell−outer shell (see Materials and Methods section for details; see the inset in Figure 1c). The SERS-active effect of gold−silver nanodumbbells was confirmed by atomic force microscope-correlated nano-Raman measurements of individual dumbbell structures. The results demonstrated that Raman signals can be repeatedly detected from single-molecule-tethered nanodumbbells.[10] Thus, the newly developed particles can be employed as programmed smart reagents for single DNA detection of pathogens, which have a promising impact on tackling the threats associated with the antibiotic resistance. Both SPION core and the intermediate gold shell have the ability to induce heat by applying alternative magnetic and laser fields, respectively. Thereby, hyperthermia can be used as additional means to escalate bacterial death using these nanoparticles. The SPR effects between the gold and silver gap can be used for higher heating capability of the silver shell.

Figure 2a−g shows representative transmission electron microscopy (TEM) images and corresponding size distribution of silver nanoparticles (Figure 2a,b), bare SPIONs (Figure 2c), SPION−silver core−shell particles (Figure 2d,g), SPION−gold core−shell particles (Figure 2e,g), and SPION−gold−silver core−intermediate shell−shell nanoparticles (Figure 2f,g). Silver nanoparticles were synthesized as control antibacterial particles in order to highlight the significance of the engineered

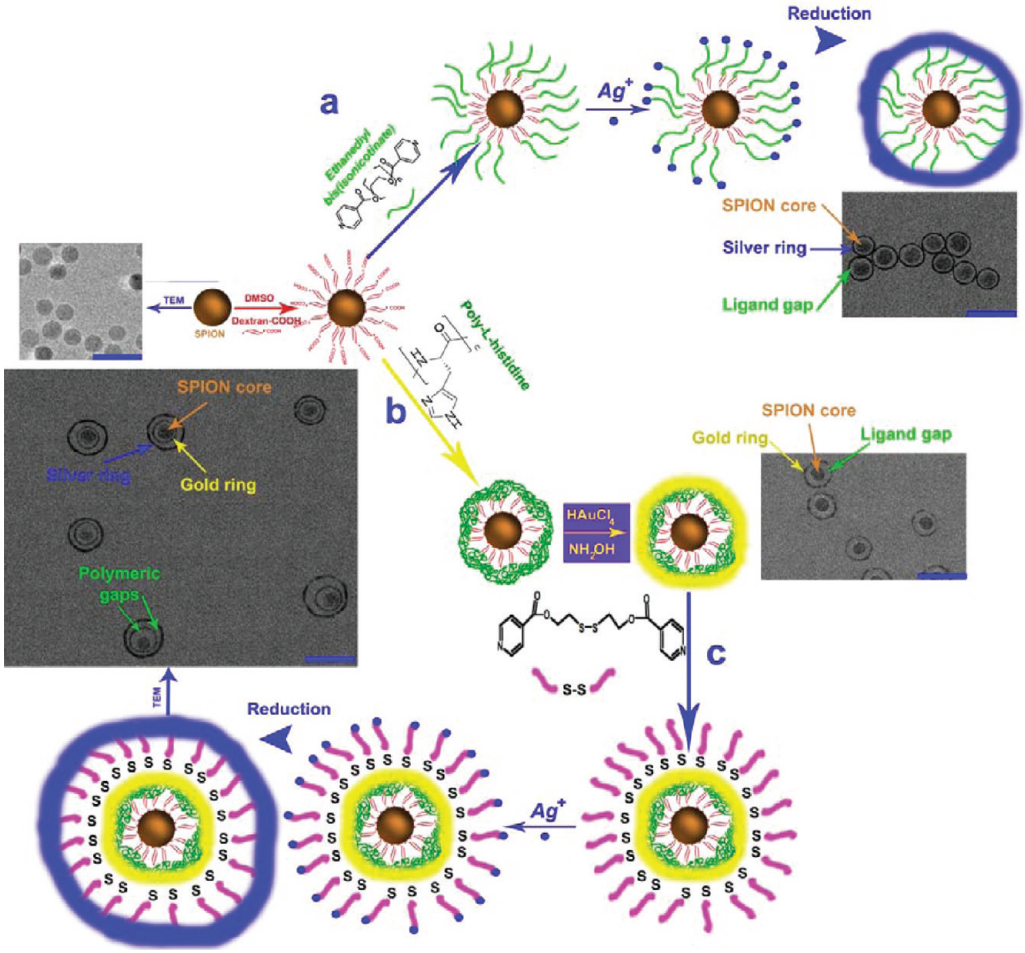

Figure 1. Schematic representation of core–shell nanoparticles with polymeric gaps. (a) Key steps involved in the synthesis of silver ring-coated SPIONs with a polymeric gap. Monodisperse SPIONs were coated with carboxylated dextran using ligand exchange followed by conjugation with ethanediylbis(isonicotinate), which is capable of chelating silver ions. Reduction of silver ions resulted in the formation of monodispersed silver ring-coated SPIONs. (b) Key steps involved in the synthesis of gold ring-coated SPIONs with a polymeric gap as the intermediate stage; PLH, which is capable of chelating gold ions, is adsorbed onto carboxylated dextran by electrostatic interaction. By addition of gold ions and a reducing reagent, thin gold shells form on the polypeptide template. (c) Surface treatment of gold core–shell nanoparticles with disulfide ethanediylbis-(isonicotinate) followed by addition of silver ions. Reduction of silver ions resulted in the formation of monodispersed silver ring-coated gold-coated SPIONs. TEM panels are representative images showing the formation of monodispersed nanoparticles in various stages (scale bars are 40 nm).

nanoparticles. TEM micrographs revealed that all of the prepared multifunctional particles were monodispersed and the shell thickness of both gold and silver rings was approximately 2–3 nm. The particles also exhibited a transparent gap with a size of ~3–5 nm between the core and shell and also between the intermediate and outer shells. Appearance of these features was due to the fact that sandwiched organic materials are not electron-dense enough for TEM visualization. The formation of ligand gaps confirmed that gold and silver shells were not deposited directly on the surface of the core but were template-coated *via* the polymer outer layer. Figure 2h shows the extinction spectra of the nanoparticles corresponding to their TEM images. The well-separated SPION–gold core–shell nanostructures observed in this study have also been reported by Jin and co-workers.[11]

It is well known that gold and silver nanoparticles show significant absorbance peaks due to their surface plasmon resonance (SPR) capability.[12] However, it has been reported that, by creating gold nanoshells, the SPR band of gold nanoparticles is transferred to the near-infrared (NIR) spectrum, based upon to the thickness of the shells (see Figure S1 of Supporting Information).[11] According to Figure 2h, the SPR peaks of both SPION–gold and silver core–shell nanoparticles were widened and transferred to the NIR region when compared with silver and gold nanoparticles alone (for the spectrum of gold nanoparticles, see ref 13). The observed peak broadening can be attributed to several factors that emerge in the core–shell particles (*e.g.*, phase retardation effects, size distribution of both cores and shells, and electron scattering at shell interfaces).[14] In contrast, in the case of SPION–gold–silver

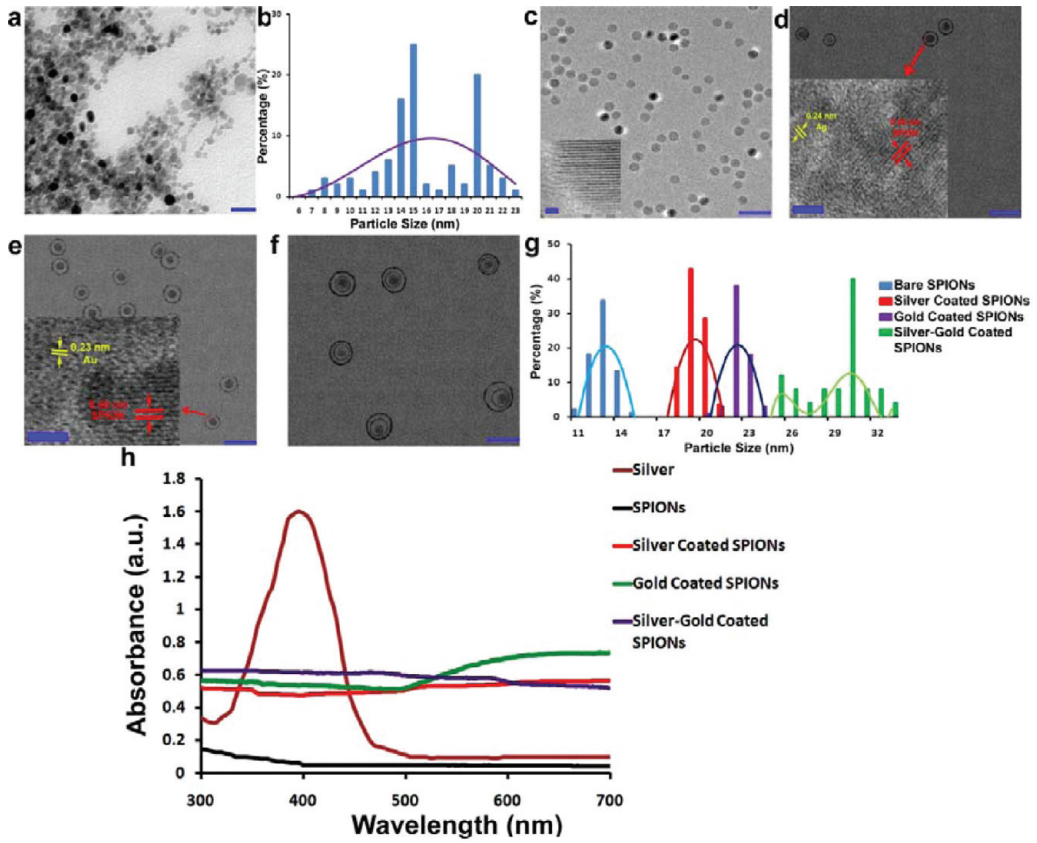

Figure 2. TEM imaging and optical properties of various nanoparticles. (a) TEM image and (b) size distribution histogram of silver nanoparticles. (c–f) TEM images of bare SPIONs, silver-coated SPIONs, gold-coated SPIONs, and silver-coated gold-coated SPIONs, respectively. The polymeric gaps are not visible under TEM because of their low electron densities. TEM scale bars are 40 nm. The inset in (c) shows high-resolution TEM image of SPIONs. The insets in (d) and (e) show high-resolution TEM images of core–shell nanoparticles. The lattice spacings of the silver and gold shells are 0.24 and 0.23 nm, respectively, for (111) crystal planes of face-centered cubic (fcc) silver and gold (the lattice spacing of the SPIONs is 0.48 nm corresponding to its (111) plane); the scale bars for panels show 1 nm. (g) Size distribution histograms of various nanoparticles; the particle size histograms are plotted from analysis of >50 particles for each sample. (h) Extinction spectra of all nanoparticles, confirming the successive coating of silver and gold shells onto polymer-coated SPIONs.

multifunctional nanoparticles, the SPR peak did not shift to lower wavelengths. This may be related to the fluorescence quenching effect that has also been detected in gold-coated quantum dots.[13]

Magnetic properties of nanoparticles were evaluated using a Quantum Design superconducting quantum interference device (SQUID). Figure 3a,b shows the hysteresis curves collected at $T = 2$ and 300 K. The low-temperature hysteresis (Figure 3a) was slightly opened with small coercive fields; however, there was no hysteresis loop for nanoparticles at 300 K, indicating the superparamagnetic properties of these particles. All of the multifunctional particles demonstrated magnetic saturation amounts adequate for particle penetration within the bacterial biofilms. Due to their higher shell thickness, the saturation magnetization of SPION–gold–silver nanoparticles was slightly lower than that in the SPION–silver particles.

Live/dead assay was conducted on *Staphylococcus epidermidis* and *Staphylococcus aureus* after 24 h of growth, in the absence or presence of various nanoparticles and antibacterial drug (kanamycin) (Figure 3c). Although the magnetic properties of SPIONs decreased as coating was applied to the particles, from bare nanoparticles to silver–gold-coated ones (Figure 3a,b), the magnetic properties of the coated SPIONs were still sufficient to enable the particles to penetrate within the film. In the presence of either SPION–silver particles or SPION–gold–silver nanoparticles, the percentage of dead bacteria in the biofilms was significantly higher than that in the presence of silver nanoparticles when the exact same particle concentration was used. Interestingly, the SPION–gold shell exhibited no differences in the percentage of dead bacteria when compared to that in the control for both bacteria types. The effect of the external magnetic field of both silver-coated SPIONs (*i.e.*, SPION–silver and SPION–gold–silver nanoparticles) on the *Staphylococcus epidermidis* and *Staphylococcus aureus* biofilms was a significant increase in the amount of dead bacteria. However, no difference was detected between nonmagnetic particles and drug-treated bacteria. There was a slight increase in the amount of dead bacteria for SPION–gold particles. This can be attributed to the penetration

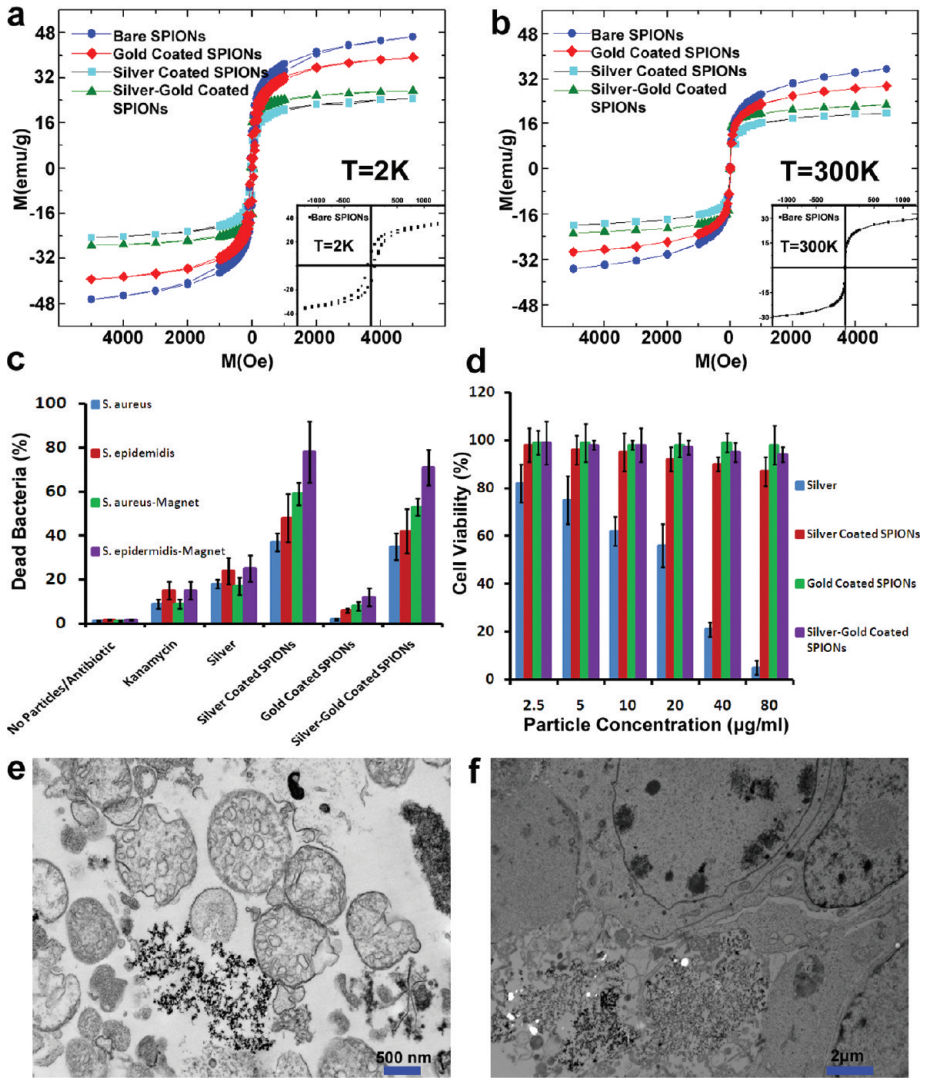

Figure 3. Dual toxicology effect of multifunctional nanoparticles in bacteria and human cells. (a,b) Magnetization *vs* magnetic field at 2 and 300 K for all nanoparticles, showing the suitable magnetic properties of antibacterial particles for penetration in biofilms; the insets show the magnified plots for the bare SPIONs. (c) Percentage of dead bacteria in 24 h old staphylococcal biofilms, with and without external magnetic field, of S. aureus and S. epidermidis in the absence and presence of various particles. Error bars represent standard deviation over 10 independent experiments. Experiments with kanamycin (antibacterial drug) were carried out on bacteria for confirmation of strong antibacterial effects of multifunctional particles. (c) Toxicity evaluation of nanoparticles interacted with HepG2 cell lines for a period of 24 h. (e,f) Transmission electron micrographs of HepG2 cells after 24 h of growth in tissue culture polystyrene wells in the presence of silver and silver–SPION core–shell particles (with the exact same concentration of nanoparticles). The electron microscopy images confirm the highly toxic effects of silver nanoparticles on the cells, while there was no sign of toxicity for silver–SPION core–shell particles.

of the nanoparticles within the biofilm and increasing their total amount in the bacteria layer.

In order to assess the toxicity effects of the manufactured nanoparticles on the cells, human liver carcinoma cell line (HepG2) was treated with various nanoparticles at different concentrations (Figure 3d). Silver nanoparticles showed significant toxicity at the highest concentration applied (metal ion concentration of 80 μg/mL). However, at the same particle concentration, SPION–silver and SPION–gold–silver nanoparticles were both fully compatible with the cells. The toxic effects of these engineered particles against bacteria together with their compatibility with human cells can introduce them as candidate nanoparticles to fight against the antibacterial resistance threat.

In order to further investigate the effect of silver and SPION–silver core–shell nanoparticles, the TEM imaging was utilized (Figure 3e,f). While silver nanoparticles demonstrated adverse effects on the HepG2 cells (Figure 3e), the cells interacting with SPION–silver particles appeared normal (Figure 3f). As can be seen in Figure 3f, the SPION–silver particles had entered into the intercellular environment *via* endocytosis (for more details, see Figures S2 and S3 of the Supporting Information).

The antibacterial activity of silver nanoparticles can be due to multiple mechanisms. The main mechanism suggested is related to the oxidative stress generated by reactive oxygen species (ROS).[15] Choi *et al.*[15] showed

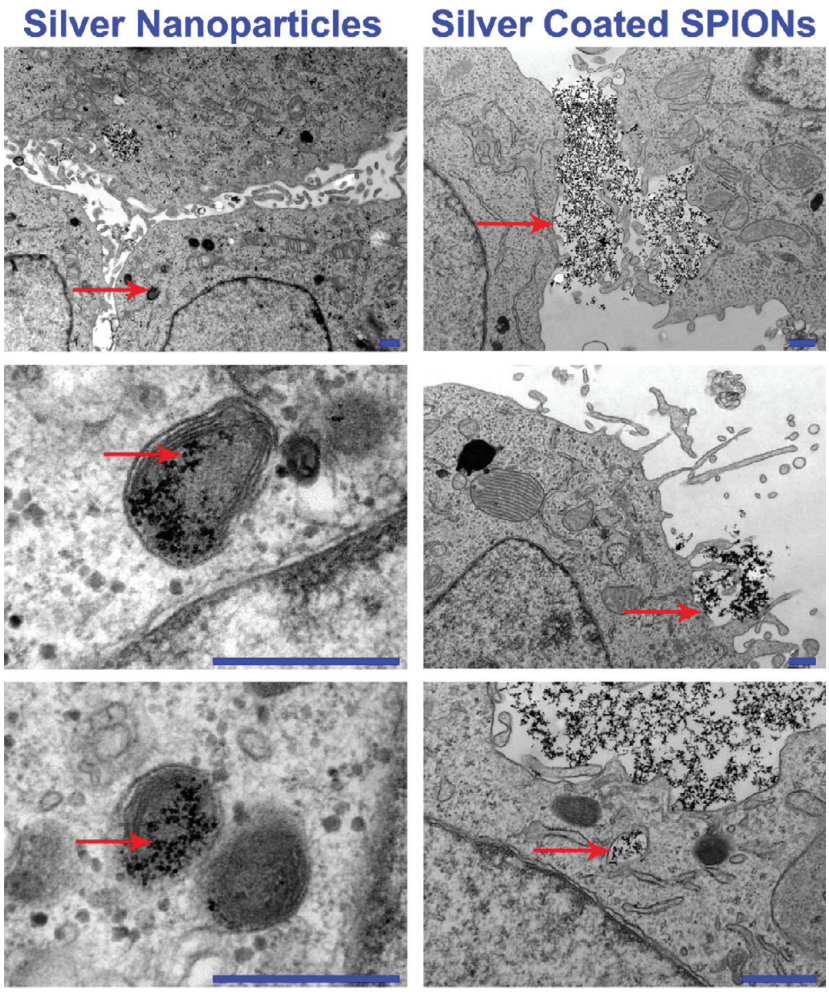

Figure 4. Transmission electron micrographs of HepG2 cells after 3 h of growth in tissue culture polystyrene wells in the presence of silver and silver–SPION core–shell particles (with the exact same concentration of nanoparticles). The images confirm the accumulation of silver nanoparticles (red arrows) in cellular mitochondria, resulting in their high toxic effects on the cells; in contrast, there were no traces of silver-coated SPIONs (red arrows) in mitochondria of cells, making them compatible with the cells (scale bars: 500 nm).

that silver nanoparticles with diameters lower than 5 nm could be more toxic to bacteria compared with the bigger ones. Similar effect can exist for the silver ring-coated nanoparticles. More specifically, these particles possess promising ability to induce oxidative stress generated by ROS. Another possible antibacterial mechanism is the electrostatic interactions between nanoparticles and bacterial cell membranes or cell membrane proteins, which can result in physical damage followed by bacteria death.[5,15] Due to their different physicochemical properties in comparison with that of silver nanoparticles, the silver ring-coated nanoparticles induce different bacterial/cellular responses. It is now well-recognized that, once nanoparticles infiltrate the biological medium, their surface gets covered by various proteins.[16,17] The composition of the associated proteins in this coating is strongly dependent on the physicochemical properties of the nanoparticles.[18] Thereupon, the altered composition of protein corona on the surface of silver ring-coated particles, in comparison to that on silver nanoparticles, results in dual toxicity effect of these particles against bacteria and cells.

In order to confirm the mentioned mechanism, we did electron microscopy analysis at the highest applied particle concentration (metal ion concentration of 80 μg/mL) at an interaction time of 3 h with cells (see Figure 4). The results confirmed the accumulation of silver nanoparticles in the mitochondria of the cells; in this case, as proposed before, the most possible mechanism of toxicity of silver nanoparticles is their ability to disrupt the mitochondrial respiratory chain, leading to production of ROS and interruption of ATP synthesis,[19] which in turn causes DNA damage. In contrast, the silver-coated SPION nanoparticles entered the intercellular medium *via* endocytosis uptake, and there is no trace of particles in the mitochondria of the cells. Thus, there are no/little amounts of ROS production, resulting in no/reversible damage to the DNA. We recently reported that small changes in the nanoparticles'

surface roughness can cause significant alterations in the protein corona composition.[20] The observed cellular trafficking variation for silver nanoparticles *versus* silver-coated SPIONs may therefore be related to their various protein corona compositions.

CONCLUSION

In this study, novel generations of antimicrobial magnetic silver ring-coated particles, consisting of superparamagnetic cores, were designed and developed. It was demonstrated that the formation of these nanoparticles strongly enhances the antimicrobial activities of silver, not only through the upregulation of ROS production in bacteria, but also by the deep penetration of the particles within bacterial biofilm using an external magnetic field. The engineered magnetic nanoparticles do not cause toxicity to the human cells, hence, introducing an efficient antimicrobial agent in treating pathogens and infections. The prospective applications of antibacterial silver ring SPIONs will entail significant consideration by the scientific community in the future.

MATERIALS AND METHODS

Materials. Oleic acid (90%) and 1-octadecene were purchased from Sigma-Aldrich (St. Louis, MO, USA). Oleyl alcohol was purchased from TCI. *n*-Hexane was purchased from Samchun Chem (Seoul, Korea). Silver nitrate, sodium borohydride, kanamycin, isonicotinic acid, dextran (average molecular weight of 5000), polyethylene glycol (PEG, average molecular weight of 400), poly(ethylene oxide) (6-arm, anthracene-terminated) with an average molecular weight of 12 000, dimethyl sulfoxide, polyvinylpyrrolidone (PVP), sodium periodate, potassium cyanide, diethylene glycol, sodium hydroxide (NaOH), $NH_2OH \cdot HCL$, gold salt ($HAuCl_4$), and poly-L-histidine (PLH) were purchased from Sigma-Aldrich (Taufkirchen, Germany). PLH was used as templates to direct gold nucleation and growth. Tryptone soy broth (TSB) was purchased from Oxoid Ltd. (Basingstoke, United Kingdom).

Synthesis of Silver Nanoparticles. Silver nanoparticles were synthesized using a standard procedure by reduction of silver nitrate.[19] Briefly, 20 mL of aqueous solution of $AgNO_3$ (1 mM) was reduced with 2 mL of 40 mM aqueous sodium citrate solution at room temperature. Subsequently, 0.5 mL of 100 mM aqueous sodium borohydride solution was added dropwise to the prepared solution under vigorous stirring, yielding a light yellow color. Then, 0.5 mL of an aqueous solution of PVP (40 mM) was added, resulting in the solution color change to a darker yellow color. This occurred after the reaction proceeded for 30 min, indicating formation of spherical silver NPs. All of the experiments were conducted in a clean atmosphere to eliminate the chances of endotoxin contamination that may interfere with the toxicity profile of the nanoparticle.[19,21]

Synthesis of Iron Oxide Nanoparticles. SPIONs were synthesized according to a previously reported procedure.[22] Briefly, iron–oleate complexes were prepared by reacting sodium oleate and iron(III) chloride. For the synthesis of SPIONs with an average size of 13 nm, 18 g (20 mmol) of iron–oleate complex and 5.7 g of oleic acid (20 mmol) were dissolved in 100 g of 1-octadecene at room temperature. The reaction mixture was degassed at 80 °C for 2 h. The mixture was heated to reflux temperature at a heating rate of 3 °C/min and then kept for 30 min under an inert atmosphere. After the reaction, the container vessel was rapidly cooled to room temperature, followed by the addition of 500 mL of acetone in order to start the SPION precipitation. The SPIONs were separated by a centrifuge and dispersed in hexane.

Preparation of the Carboxylated Dextran. Carboxylated dextran was prepared according to the procedure reported elsewhere.[23] At first, the hydroxyl groups in dextran were oxidized to aldehyde groups using sodium periodate.[24] Briefly, sodium periodate was dissolved in deoxygenated DI water and introduced to dextran (molecular average weight of 5000) solution (4 g in 30 mL of deoxygenated DI water). The solution was homogenized for 2 h at room temperature followed by dialyzing with a membrane bag (1000 cutoff molecular weight) for 4 days. Cyanohydrin intermediate was prepared *via* an interaction between the obtained solution and potassium cyanide. Finally, carboxylic acid groups were created at the terminal units of dextran through the hydrolysis of the obtained cyanohydrin intermediate. Prepared carboxylated dextran was lyophilized and stored at −80 °C.

Carboxylated Dextran-Coated SPIONs. In order to coat the prepared hydrophobic SPIONs with carboxylated dextran, the ligand exchange process was employed.[25,26] In this case, SPIONs at iron concentrations of 1 mg/mL were produced and mixed with the dextran ligands in DMSO (a dipolar solvent). The reactions between the nanoparticles and polymer were conducted at room temperature (for 72 h) while shaking in the incubator. DMSO can make homogeneous solutions with both aqueous polymer substrates and organic solvents.[25] Next, 1 mL of stock SPION solution was mixed with carboxylated dextran in 30 mL of DMSO. Once the reaction was complete, coated SPIONs were magnetically collected through a strong magnetic field using a magnetic-activated cell sorting (MACS) system and redispersed into 1 mL of DI water. These water-soluble SPIONs were completely stable at room temperature without detectable precipitation.

Synthesis of the Smooth Silver Ring-Coated SPIONs with a Ligand Gap. In order to deposit a silver ring shell on the surface of carboxylate-coated SPIONs with a ligand gap, ethanediylbis-(isonicotinate) (prepared according to the previous report by Gordon *et al.*[27]) was utilized to interact with the silver ions. Ethanediylbis(isonicotinate), derived from biocompatible components isonicotinic acid and polyethylene glycol (PEG) units,[28] was added to the carboxylate-coated SPIONs (0.5 μM) for 20 min, and the obtained particles were collected by MACS system followed by several rinses with DI water. The accumulated particles were redispersed in the DI water containing silver nitride (1 μM) and mixed for additional 20 min. Subsequently, particles were separated again by MACS. For the preparation of the silver ring shell, the silver ions which were linked to ethanediylbis(isonicotinate)-coated SPIONs, were reduced by redispersion of the particles in DI water containing sodium borohydride. The obtained silver ring-coated SPIONs with a ligand gap were fixed in the MACS system and washed by DI water. After redispersion in DI water, the produced particles were stored at 2–8 °C. It is notable that the zeta-potential of the particles was −12 mV.

Synthesis of the Smooth Gold Ring-Coated SPIONs with a Ligand Gap. Smooth gold shell SPIONs were produced according to a previous report.[11] Briefly, carboxylated dextran-coated SPIONs were immersed in PLH at the pH of 5–6 (pH adjustment was done using 0.1 N HCl). After incubation for 60 min, the coated SPIONs were collected using a magnet and rinsed several times by DI water. The obtained solution was mixed with $HAuCl_4$ (1% w/w) for 20 min, with the pH being adjusted to 9–10 using NaOH. Subsequently, $NH_2OH \cdot HCL$ was added to the solution, as reducing agent, and mixed well until the color of the colloidal suspension turned dark blue. The color change was visible within a few minutes. The solution was then washed several times, redispersed in DI water using a sonicator, and stored at 2–8 °C for the silver coating process.

Synthesis of the Smooth Silver-Coated Gold Ring-Coated SPIONs with Double Ligand Gap. The gold ring-coated SPIONs with ligand gaps

were collected by the MACS system and redispersed in 5 mL of disulfide solution (5 mM bis 2-((4-pyridinylcarbonyl)oxy)ethyl disulfide (prepared according to the previous report by Slenters *et al.*[29]) dissolved in 100 mL of CH_2Cl_2/EtOH (1:1)) and mixed well for 5 h. The gold-coated particles were fixed in MACS, rinsed with EtOH, and immediately redispersed in ethanediylbis-(isonicotinate) 0.5 μM solution. After homogenization for 20 min, the particles were collected by MACS and redispersed in DI water solution containing silver nitride. This was followed by homogenization for an additional 20 min. Processed particles were collected by MACS and washed several times by DI water and reduced by redispersion of the particles in DI water containing sodium borohydride. The obtained silver ring−shell-coated gold intermediate−shell SPIONs with double ligand gaps were fixed in MACS and washed by DI water followed by a redispersion in DI water and storage at 2−8 °C for future work.

Characterizations of Nanoparticles. Size and shape of the produced nanoparticles were evaluated by using a Phillips CM200 transmission electron microscope (TEM; Eindhoven, The Netherlands). To prepare samples for TEM, a drop of the suspension was placed on a copper grid and dried. Magnetization measurements were performed on solid samples (dry powder) using a Quantum Design superconducting quantum interference device MPMS-XL7 magnetometer. Hysteresis experiments in the range of $-5\ T \leq H \leq +5\ T$ were conducted at $T = 300$ K. In order to characterize absorption spectra of nanoparticles, UV/vis spectroscopy of the samples was performed using a Lambda 950 spectrophotometer (PerkinElmer, USA) from 300 to 700 nm wavelengths.

Growth of Adhering Bacteria in the Absence and Presence of Various Nanoparticles. *Staphylococcus aureus* (ATCC 19636) and *Staphylococcus epidermidis* (ATCC 35984) were employed for the evaluation of the antibacterial effects of various particles. Staphylococci were first grown aerobically overnight at 37 °C on blood agar from a frozen stock. The plate was kept at 4 °C. For each experiment, one colony was inoculated in 10 mL of TSB and cultured for 16 h. Bacteria were harvested by centrifugation at 5000*g* for 5 min at 10 °C and washed with sterile PBS. They were suspended in TSB to a concentration of 10^5 bacteria/mL.

One hundred microliters of bacterial suspension was put in each well of polystyrene 96-well plates (NUNC MaxiSorp, Nunc A/S, Roskilde, Denmark) in the absence or presence of various particles. The total metal ion concentration (*i.e.*, the concentration of Ag ions for silver nanoparticles, or the sum of Ag, Au, and Fe ion concentrations for silver ring/gold shell SPIONs) of 80 μg/mL was used. Bacteria were allowed to grow aerobically at 37 °C for 24 h. In addition to the role of particles, the effect of 1 μg of addition of kanamycin, an aminoglycoside antibiotic used for the treatment of a wide variety of infections, was examined.

Subsequently, wells were rinsed with PBS, and unbound bacteria were removed. In order to assess the viability of adhering staphylococci after 24 h of the biofilm growth, LIVE/DEAD*Bac*Ligh bacterial viability kit (Molecular Probes Inc., Oregon,USA) was employed. The kit consists of two probes: SYTO9 is a membrane-permeated nucleic acid stain (green fluorescence at 530 nm upon excitation at 488 nm) that labels the living bacteria. The second probe is propidium iodide (PI, red fluorescence at 620 nm upon excitation at 488 nm) and enters only the bacteria with compromised membranes. After staining with the kit, the plates were incubated for 15 min in the dark at room temperature. The fluorescence intensities were measured by using a 96-well fluorescence microplate reader. Measurements were performed 10 times on separately cultured bacteria.

Penetration of Magnetic Particles during Biofilm Growth. Each well of the 96-well plates was filled with 100 μL of either *Staphylococcus aureus* or *Staphylococcus epidermidis* suspensions. The bacteria were allowed to adhere and grow aerobically at 37 °C for 24 h in the absence or presence of various nanoparticles. An external magnetic field was applied by placing the plates on top of a strong permanent magnet. Subsequently, wells were rinsed with PBS, and unbound bacteria were removed. The bacteria viability was assessed using the LIVE/DEAD assay as described in the previous section. Experiments were repeated 10 times using separately cultured bacteria.

***In Vitro* Biocompatibility Assessment.** Human liver carcinoma cell line (HepG2 (ATCC HB-8065)) was seeded on 96-well plates at 10 000 cells per well in 150 μL of medium and incubated for 24 h. Cells were cultured in Dulbecco's modified Eagle's medium (DMEM) supplemented with 10% fetal bovine serum (FBS) at 37 °C in a 5% CO_2 incubator. After the 24 h incubation period, 40 μL of medium containing various nanoparticles (with total metal ions concentration of 80 μg/mL) was added to each well, and cells were incubated for an additional 24 h. Control cells were incubated with the same culture medium without the nanoparticles. Different particle concentrations and controls were each seeded in 10 separate wells. Cytotoxicity of the nanoparticles was assessed using the modified MTT (3-(4,5-dimethylthiazol-2-yl)-2,5-diphenyltetrazolium bromide) assay.[30,31] After 24 h of incubation of the cell with or without the nanoparticles, 100 μL of MTT (0.5 mg/mL) was added to each well. Following 3 h incubation, the medium was removed and formazan crystals were solubilized by incubation in 150 μL of isopropyl alcohol for 20 min. The absorbance of each well, as an indicator of the cell viability, was read at 545 nm using a microplate reader (Stat Fax-2100, Awareness, Palm City, FL).

Statistics. Live/Dead and MTT assays were performed in 10 separate experiments, with the results expressed as mean ± standard deviation. The standard deviation values are indicated as error bars in the result plots. The results were statistically processed for outlier detection using a "T procedure"[32] using MINITAB software (Minitab Inc., State College, PA). One-way analysis of variance (ANOVA) with $p < 0.05$ was performed for each set of test repeats. Outlier samples were excluded from the corresponding assay viability calculations.

Conflict of Interest: The authors declare no competing financial interest.

Supporting Information Available: Additional figures. This material is available free of charge *via* the Internet at http://pubs.acs.org.

REFERENCES AND NOTES

1. http://ec.europa.eu/research/leaflets/antibiotics.
2. Gristina, A. Biomaterial-Centered Infection: Microbial Adhesion *versus* Tissue Integration. *Science* **1987**, *237*, 1588–1595.
3. Khalil, H.; Williams, R. J.; Stenbeck, G.; Henderson, B.; Meghji, S.; Nair, S. P. Invasion of Bone Cells by *Staphylococcus epidermidis*. *Microbes Infect.* **2007**, *9*, 460–465.
4. Mahmoudi, M.; Azadmanesh, K.; Shokrgozar, M. A.; Journeay, W. S.; Laurent, S. Effect of Nanoparticles on the Cell Life Cycle. *Chem. Rev.* **2011**, *111*, 3407–3432.
5. Liu, L.; Xu, K.; Wang, H.; Jeremy Tan, P. K.; Fan, W.; Venkatraman, S. S.; Li, L.; Yang, Y.-Y. Self-Assembled Cationic Peptide Nanoparticles as an Efficient Antimicrobial Agent. *Nat. Nanotechnol.* **2009**, *4*, 457–463.
6. Rai, M.; Yadav, A.; Gade, A. Silver Nanoparticles as a New Generation of Antimicrobials. *Biotechnol. Adv.* **2009**, *27*, 76–83.
7. Hussain, S. M.; Hess, K. L.; Gearhart, J. M.; Geiss, K. T.; Schlager, J. J. *In Vitro* Toxicity of Nanoparticles in BRL 3A Rat Liver Cells. *Toxicol. in Vitro* **2005**, *19*, 975–983.
8. Carlson, C.; Hussain, S. M.; Schrand, A. M.; Braydich-Stolle, L. K.; Hess, K. L.; Jones, R. L.; Schlager, J. J. Unique Cellular Interaction of Silver Nanoparticles: Size-Dependent Generation of Reactive Oxygen Species. *J. Phys. Chem. B* **2008**, *112*, 13608–13619.
9. Fabrega, J.; Renshaw, J. C.; Lead, J. R. Interactions of Silver Nanoparticles with *Pseudomonas putida* Biofilms. *Environ. Sci. Technol.* **2009**, *43*, 9004–9009.
10. Lim, D.-K.; Jeon, K.-S.; Kim, H. M.; Nam, J.-M.; Suh, Y. D. Nanogap-Engineerable Raman-Active Nanodumbbells for Single-Molecule Detection. *Nat. Mater.* **2010**, *9*, 60–67.
11. Jin, Y.; Jia, C.; Huang, S. W.; O'Donnell, M.; Gao, X. Multifunctional Nanoparticles as Coupled Contrast Agents. *Nat. Commun.* **2010**, *1*, 1–8.
12. Hutter, E.; Fendler, J. H.; Roy, D. Surface Plasmon Resonance Studies of Gold and Silver Nanoparticles Linked to Gold and Silver Substrates by 2-Aminoethanethiol and 1,6-Hexanedithiol. *J. Phys. Chem. B* **2001**, *105*, 11159–11168.

13. Jin, Y.; Gao, X. Plasmonic Fluorescent Quantum Dots. *Nat. Nanotechnol.* **2009**, *4*, 571–576.
14. Park, J.; Joo, J.; Kwon, S. G.; Jang, Y.; Hyeon, T. Synthesis of Monodisperse Spherical Nanocrystals. *Angew. Chem., Int. Ed.* **2007**, *46*, 4630–4660.
15. Choi, O.; Hu, Z. Size Dependent and Reactive Oxygen Species Related Nanosilver Toxicity to Nitrifying Bacteria. *Environ. Sci. Technol.* **2008**, *42*, 4583–4588.
16. Monopoli, M. P.; Walczyk, D.; Campbell, A.; Elia, G.; Lynch, I.; Baldelli Bombelli, F.; Dawson, K. A. Physical−Chemical Aspects of Protein Corona: Relevance to *In Vitro* and *In Vivo* Biological Impacts of Nanoparticles. *J. Am. Chem. Soc.* **2011**, *133*, 2525–2534.
17. Walczyk, D.; Bombelli, F. B.; Monopoli, M. P.; Lynch, I.; Dawson, K. A. What the Cell "Sees" in Bionanoscience. *J. Am. Chem. Soc.* **2010**, *132*, 5761–5768.
18. Mahmoudi, M.; Lynch, I.; Ejtehadi, M. R.; Monopoli, M. P.; Bombelli, F. B.; Laurent, S. Protein−Nanoparticle Interactions: Opportunities and Challenges. *Chem. Rev.* **2011**, *111*, 5610–5637.
19. AshaRani, P. V.; Mun, G. C. K.; Hande, M. P.; Valiyaveettil, S. Cytotoxicity and Genotoxicity of Silver Nanoparticles in Human Cells. *ACS Nano* **2009**, *3*, 279–290.
20. Mahmoudi, M.; Serpooshan, V. Large Protein Absorptions from Small Changes on the Surface of Nanoparticles. *J. Phys. Chem. C* **2011**, *115*, 18275–18283.
21. Vallhov, H.; Qin, J.; Johansson, S. M.; Ahlborg, N.; Muhammed, M. A.; Scheynius, A.; Gabrielsson, S. The Importance of an Endotoxin-Free Environment during the Production of Nanoparticles Used in Medical Applications. *Nano Lett.* **2006**, *6*, 1682–1686.
22. Park, J.; An, K.; Hwang, Y.; Park, J.-G.; Noh, H.-J.; Kim, J.-Y.; Park, J.-H.; Hwang, N.-M.; Hyeon, T. Ultra-Large-Scale Syntheses of Monodisperse Nanocrystals. *Nat. Mater.* **2004**, *3*, 891–895.
23. Usher, T. C.; Wallis, S. H. Process of Making Carboxilated Dextran. U.S. Patent US6 703 499, 2004.
24. Martwiset, S.; Koh, A. E.; Chen, W. Nonfouling Characteristics of Dextran-Containing Surfaces. *Langmuir* **2006**, *22*, 8192–8196.
25. Xu, Y.; Qin, Y.; Palchoudhury, S.; Bao, Y. Water-Soluble Iron Oxide Nanoparticles with High Stability and Selective Surface Functionality. *Langmuir* **2011**, *27*, 8990–8997.
26. Mahmoudi, M.; Amiri, H.; Shokrgozar, M. A.; Sasanpour, P.; Rashidian, B.; Laurent, S.; Casula, M. F.; Lascialfari, A. Raman Active Jagged-Shaped Gold-Coated Magnetic Particles as a Novel Multimodal Nanoprobe. *Chem. Commun.* **2011**, *47*, 10404–10406.
27. Gordon, O.; Vig Slenters, T.; Brunetto, P. S.; Villaruz, A. E.; Sturdevant, D. E.; Otto, M.; Landmann, R.; Fromm, K. M. Silver Coordination Polymers for Prevention of Implant Infection: Thiol Interaction, Impact on Respiratory Chain Enzymes, and Hydroxyl Radical Induction. *Antimicrob. Agents Chemother.* **2010**, *54*, 4208–4218.
28. Slenters, T. V.; Hauser-Gerspach, I.; Daniels, A. U.; Fromm, K. M. Silver Coordination Compounds as Light-Stable, Nano-Structured and Antibacterial Coatings for Dental Implant and Restorative Materials. *J. Mater. Chem.* **2008**, *18*, 5359–5362.
29. Brunetto, P. S.; Slenters, T. V.; Fromm, K. M. *In Vitro* Biocompatibility of New Silver(I) Coordination Compound Coated-Surfaces for Dental Implant Applications. *Materials* **2011**, *4*, 355–367.
30. Mahmoudi, M.; Simchi, A.; Imani, M.; Milani, S. A.; Strove, P. An *In Vitro* Study of Bare and Poly(ethylene glycol)-*co*-Fumarate-Coated Superparamagnetic Iron Oxide Nanoparticles: A New Toxicity Identification Procedure. *Nanotechnology* **2009**, *20*, 225104.
31. Mahmoudi, M.; Simchi, A.; Imani, M.; Shokrgozar, M. A.; Milani, A. S.; Häfeli, U. O.; Stroeve, P. A New Approach for the *In Vitro* Identification of the Cytotoxicity of Superparamagnetic Iron Oxide Nanoparticles. *Colloids Surf., B* **2010**, *75*, 300–309.
32. Bolton, S. *Pharmaceutical Statistics: Practical and Clinical Applications*, 2nd ed.; Marcel Dekker: New York, 1990.